

Versatile rattle-type magnetic mesoporous silica spheres, working as adsorbents and nanocatalyst containers

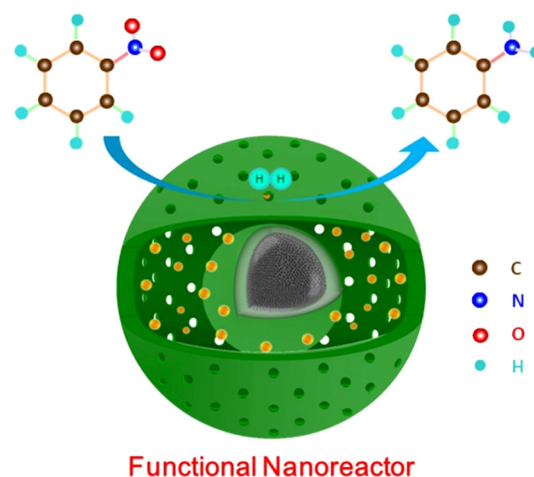
Changzi Jin^{1,2} · Yanjie Wang¹ · Hailian Tang¹ · Kaixin Zhu¹ · Xin Liu^{1,2} · Junhu Wang^{1,2}

Received: 11 May 2015 / Accepted: 4 August 2015 / Published online: 11 August 2015
© Springer Science+Business Media New York 2015

Abstract The well-defined rattle-type magnetic silica nanocomposite had been synthesized through a facile sol-gel process accompanied by a hard-template method. Structural characterizations indicated that the fabricated nanocomposite, denoted as $\gamma\text{-Fe}_2\text{O}_3\text{@SiO}_2\text{-@mSiO}_2$, was composed of nonporous silica-coating magnetic iron oxide encapsulated in mesoporous silica hollow sphere. The textural parameters of the nanocomposite are adjustable by controlling the preparation conditions. The unique structure of the prepared nanocomposite showed relatively high methylene blue adsorption capability and can be used for removal of dye from aqueous solution. In addition, some active metallic nanoparticles (such as Pt, Pd) can be introduced into the cavity of $\gamma\text{-Fe}_2\text{O}_3\text{@SiO}_2\text{-@mSiO}_2$ to construct confined integrated catalytic system. The designed Pt-based integrated nanocatalyst exhibited not only high activity and selectivity, but also an excellent reusability for the selective hydrogenation of nitrobenzol to aniline. The existence of magnetic core in the nanocomposite provides a facile separation from liquid solution.

Graphical Abstract Rattle-type nanocomposite with nonporous silica-coating magnetic iron oxide nanoparticles encapsulated in mesoporous silica hollow sphere had been prepared. This unique nanocomposite exhibits excellent adsorption capability for methylene blue dye. After loaded

with Pt nanoparticles, the formed functional nanoreactor is very active for selective hydrogenation of nitrobenzol to aniline and shows outstanding reusability.



Keywords Rattle-type · Mesoporous silica · Sol-gel process · Adsorption study · Catalysis

1 Introduction

In the past few years, mesoporous silica spheres with hollow interiors have gained more and more attention [1–4]. Compared with conventional mesoporous silica materials such as MCM-41 and SBA-15, hollow mesoporous silica spheres possess some special properties, including low density, large specific surface area and high adsorption capacity and permeability, which endow them with promising applications in catalysis, adsorption, drug

✉ Changzi Jin
jinchangzi@dicp.ac.cn

✉ Junhu Wang
wangjh@dicp.ac.cn

¹ Laboratory of Catalysts and New Materials for Aerospace, Dalian Institute of Chemical Physics, Chinese Academy of Sciences, 457 Zhongshan Road, Dalian 116023, China

² Mössbauer Effect Data Center, Dalian, China

storage and delivery [5–10]. Magnetic silica nanocomposites comprising magnetic iron oxides nanoparticles (Fe_3O_4 and $\gamma\text{-Fe}_2\text{O}_3$) and mesoporous silica can combine their respective merits and exhibit high drug-loading and targeted delivery properties in biomedicine [11–14]. In addition, due to the existence of magnetic components, the nanocomposites can be conveniently separated and recovered with the help of external magnetic field, which is significant in many applications.

To date, a large number of magnetic silica nanocomposites have been synthesized, including the core–shell structure of magnetic iron oxides coated by mesoporous silica shell and conventional mesoporous silica materials with embedded magnetic nanoparticles [15–20]. However, considering the advantages of hollow mesoporous silica aforementioned, it will be more meaningful that constructing nanocomposites with magnetic cores exist in the cavities of hollow mesoporous silica spheres, namely the rattle-type magnetic mesoporous silica nanocomposites [6, 9, 12, 21–24]. Shi's group prepared for the first time the uniform rattle-type magnetic hollow mesoporous silica spheres through sol–gel reactions followed by hydrothermal treatment and H_2 reduction [23]. Though the material has high drug storage capacity and sustained release property, the interior space of the nanocomposite from their preparation method is tiny and is not easily adjustable. Zhang et al. [21] reported the preparation of rattle-type magnetic hollow mesoporous organosilica spheres with controllable structural parameters. However, their method needed to use the organic solvent of chloroform and fluorocarbon surfactant, which limited the large-scale synthesis. Zhu et al. [24] synthesized the rattle-type $\text{Fe}_3\text{O}_4@ \text{SiO}_2$ mesoporous spheres through a facile “sacrificial templating” route, which is very efficient to produce hollow structure. However, the interior Fe_3O_4 core of their composite is unprotected. According to our previous report [16], only the porous silica shell cannot prevent the iron oxide core dissolving in acid media, which led the applications of such kind of rattle-type nanocomposites to be confined to some fields. Therefore, it remains to be interest and challenge to prepare versatile rattle-type magnetic mesoporous silica spheres through facile and effective process. Yue et al. [25] recently had reported magnetic core–shell mesoporous silica composite and further constructed Au-based catalyst. However, no research was performed about the composite's adsorption capability.

In this paper, uniform rattle-type magnetic silica nanocomposites with a layer of dense silica-coating iron oxide particles encapsulated in mesoporous silica hollow spheres were prepared by using magnetic silica/resorcinol–formaldehyde (RF) resin polymer as sacrificial template. The template of magnetic silica/RF sphere with double-layered core–shell structure was prepared through extended

Stöber method. The interior space volume of final rattle-type magnetic nanocomposite is readily adjustable. Such versatile nanocomposite not only acts as catalyst support to construct functional nanoreactor, but also exhibits high dye adsorption capacity.

2 Experimental

2.1 Chemicals

Tetraethylorthosilicate (TEOS), cetyltrimethylammonium bromide (CTAB), resorcinol, ammonia (25–28 %), ferric chloride hexahydrate ($\text{FeCl}_3 \cdot 6\text{H}_2\text{O}$), sodium acetate (NaAc), ethanol and ethylene glycol were purchased from Tianjin Kermel Chemical Company. Formaldehyde solution (37–40 %) and sodium citrate dihydrate were purchased from Tianjin Damao Chemical Company. Dihydrogen hexachloroplatinate ($\text{H}_2\text{PtCl}_6 \cdot 6\text{H}_2\text{O}$, 99.9 %) was obtained from Sigma-Aldrich. All the chemicals were of analytical grade and used as-received without purification.

2.2 Synthesis of the materials

2.2.1 Magnetite particles (Fe_3O_4)

The water-dispersible magnetite particles were prepared through solvothermal method according to previous reports [26, 27].

2.2.2 Magnetic SiO_2/RF resin polymer template

The core–shell magnetic SiO_2/RF resin polymer template, denoted as $\gamma\text{-Fe}_2\text{O}_3@ \text{SiO}_2/\text{RF}$, was prepared through a controllable extended sol–gel (Stöber) method [27]. Briefly, 140 mg magnetite particles were dispersed in 60 mL water and ethanol (volume ratio = 1:3), followed by the addition of 1 mL ammonia. After that, 0.2 g TEOS, 0.2 g resorcinol and 0.3 g formaldehyde solution were added into the mixture in turn under mechanical stirring. The obtained mixture was continuously stirred at 30 °C for 24 h and then was transferred into Teflon-lined stainless-steel autoclave and heated at 100 °C for another 24 h. The product was collected by an external magnet and washed with water and ethanol and dried at 80 °C.

2.2.3 Rattle-type magnetic mesoporous silica spheres

A total of 0.2 g $\gamma\text{-Fe}_2\text{O}_3@ \text{SiO}_2/\text{RF}$ template was dispersed in the solution containing 100 mL water, 60 mL ethanol, 0.1 g CTAB and 2 mL ammonia. Then, 0.2 g TEOS was added, and the obtained mixture was

mechanically stirred at 40 °C for the overnight. The solid product was magnetically collected and dried at 80 °C and further calcined at 500 °C in air for 4 h to remove organics. The obtained rattle-type magnetic mesoporous silica spheres are denoted as $\gamma\text{-Fe}_2\text{O}_3\text{@SiO}_2\text{-@mSiO}_2$.

2.2.4 Magnetic catalytic system

To prepare magnetic catalyst system, 0.2 g $\gamma\text{-Fe}_2\text{O}_3\text{@SiO}_2\text{@RF}$ template was firstly dispersed in 100 mL water containing 0.023 mmol H_2PtCl_6 , and the solution was vigorously stirred at 60 °C for 3 h to allow adsorption of the platinum species onto the polymer surfaces. Then, the Pt-loading template was magnetically recovered and further coated by mesoporous silica shell through a same process as $\gamma\text{-Fe}_2\text{O}_3\text{@SiO}_2\text{-@mSiO}_2$ described above. After calcination at 500 °C, the sample was reduced by 10 % H_2 and 90 % He at 250 °C for 1 h. The finally obtained catalyst system is denoted as $\gamma\text{-Fe}_2\text{O}_3\text{@SiO}_2\text{-Pt@mSiO}_2$. ICP analysis shows that the Pt amount of the catalyst is 1.29 %.

2.3 Characterization

Powder X-ray diffraction (XRD) patterns were recorded on a PANalytical X'Pert PRO powder X-ray diffractometer with Cu K α radiation. Transmission electron microscopy (TEM) images were taken on a Tecnai G2 Spirit electronic microscope with an accelerating voltage of 120 kV. Scanning electron microscopy (SEM) images were obtained on JSM-7800F field emission electron microscope. N_2 physical adsorption–desorption isotherm was measured on a Micromeritics ASAP 1020 apparatus. The samples were degassed at 350 °C for 4 h before the measurement. The platinum amounts of composite catalysts were measured by inductively coupled plasma spectrometry (ICP) on an IRIS Intrepid II XSP instrument. The phase of magnetic core was confirmed by ^{57}Fe Mössbauer spectroscopy recorded at room temperature with the use of ^{57}Co (Rh) source. All spectra were computer-fitted to a Lorentzian shape with a least-squares fitting procedure.

2.4 Adsorption tests

A total of 20 mg adsorbent was dispersed into 50 mL methylene blue (MB) aqueous solution with different concentrations. Then the solution was stirred at room temperature for a period of time, and its concentration was monitored by UV–Vis spectrometer with absorbance at wavelength of 664 nm. For pH-dependent experiments, the pH value of dye solution was adjusted by 0.1 M NaOH aqueous solution. The removal rate (R) and adsorption amounts (Q) were calculated by followed equations:

$$R = \frac{C_0 - C_t}{C_0} \times 100\% \quad (1)$$

$$Q = \frac{(C_0 - C_t)V}{M} \quad (2)$$

where C_0 and C_t are the MB concentrations of dye solution in the beginning and after a period of time, respectively. V is the volume of dye solution, and M is the mass of adsorbent.

2.5 Catalytic tests

Hydrogenation of nitrobenzene to aniline was performed in Teflon-lined autoclave (50-mL capacity). Typically, 5 mL solution of nitrobenzene in ethanol (0.1 M) and 40 mg catalyst were added into the autoclave. Then the autoclave was swept by H_2 to remove the air and sealed with H_2 pressure at 0.3 MPa. Subsequently, the reaction mixture was stirred at 40 °C for 30 min. The reaction products were analyzed by means of GC Agilent 6890 equipped with a HP-5 capillary column and a FID detector. The catalysts were magnetically recovered and thoroughly washed with ethanol for recycle tests.

3 Results and discussion

3.1 Synthesis and characterization

Figure 1 describes the synthesis procedure of rattle-type magnetic mesoporous silica spheres. Firstly, core–shell

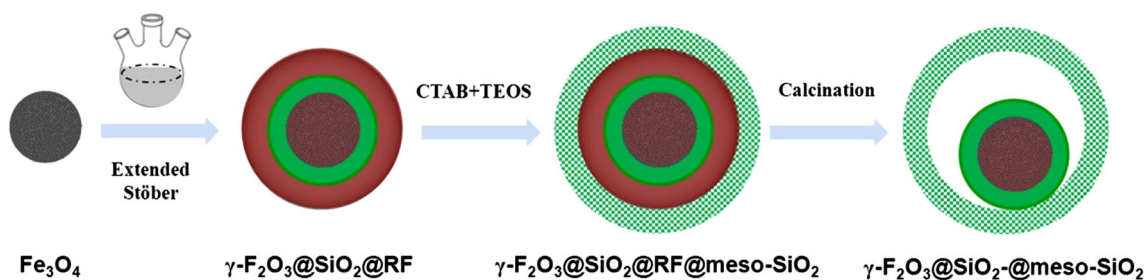


Fig. 1 Schematic representation for the preparation of rattle-type $\gamma\text{-Fe}_2\text{O}_3\text{@SiO}_2\text{-@mSiO}_2$

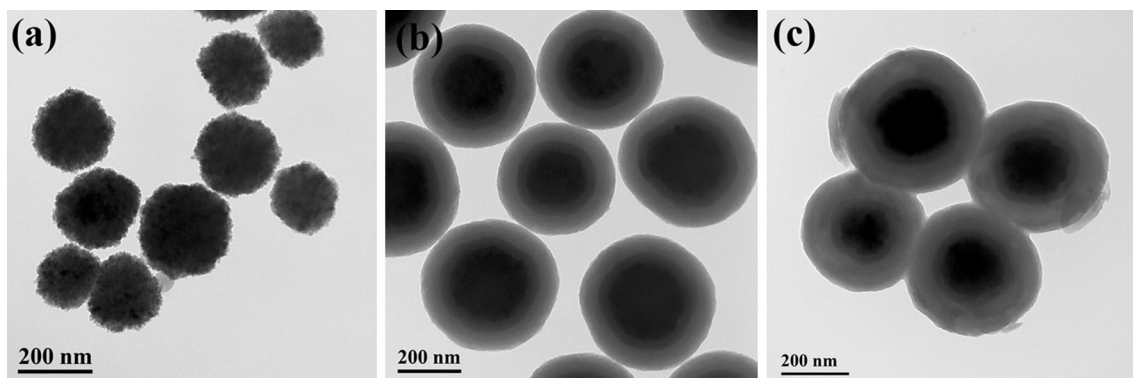


Fig. 2 TEM images of **a** magnetite particles, **b** $\gamma\text{-Fe}_2\text{O}_3@SiO_2@RF$ and **c** $\gamma\text{-Fe}_2\text{O}_3@SiO_2@RF@mSiO_2$

magnetic silica/polymer sphere $\gamma\text{-Fe}_2\text{O}_3@SiO_2@RF$ was prepared through sol–gel process, namely the so called extended Stöber method. During this process, the initial Fe_3O_4 core was oxidized into $\gamma\text{-Fe}_2O_3$, which was already demonstrated by our previous reports [16, 27]. Then, the $\gamma\text{-Fe}_2O_3@SiO_2@RF$ was further coated by mesostructural silica shell with CTAB as the template of mesopores. Finally, the as-prepared composite system was calcined to remove the organics, including the surfactant and middle

RF shell, namely the sacrificed template for the hollow cavity of final product.

Figures 2 and 3 present the TEM and SEM images of samples at different preparation stages. It is obvious that all materials show spherical morphology, including the initial Fe_3O_4 core (Fig. 2a). The $\gamma\text{-Fe}_2O_3@SiO_2@RF$ possesses clear core–shell architecture with double-layered shell composed of nonporous silica and RF polymer [27]. After mesoporous silica coating, the composite shows

Fig. 3 TEM (a, b) and SEM (c, d) images of $\gamma\text{-Fe}_2O_3@SiO_2@mSiO_2$

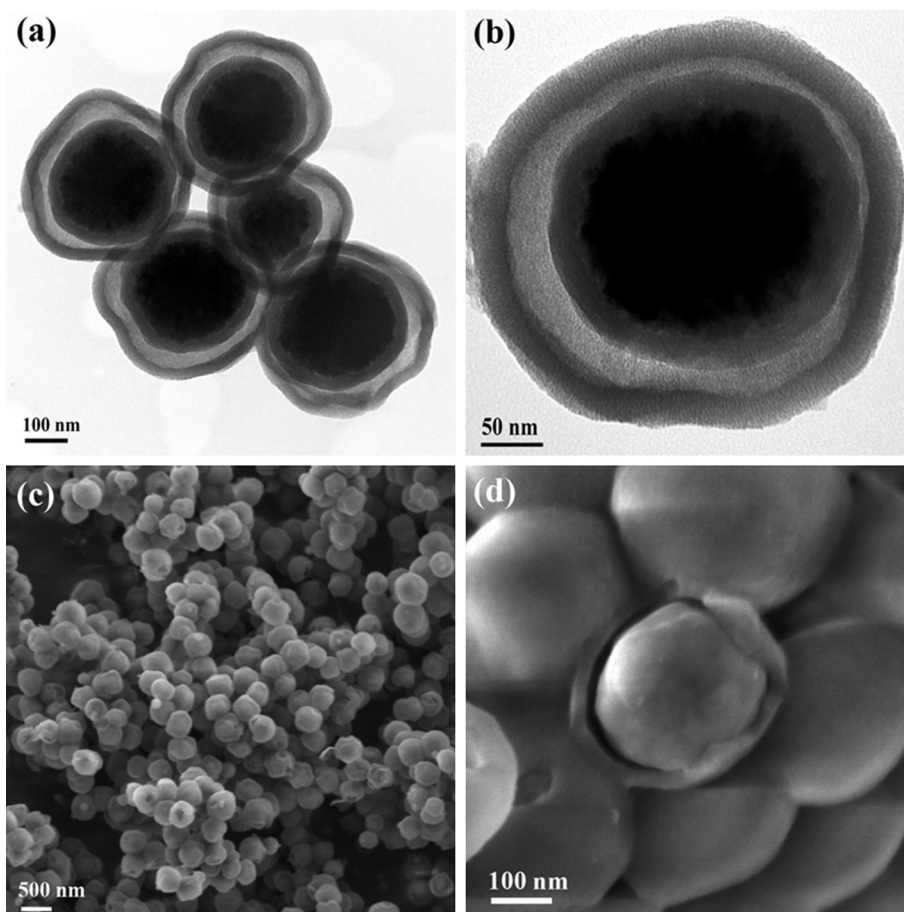


Fig. 4 TEM images of γ - $\text{Fe}_2\text{O}_3@ \text{SiO}_2\text{-@mSiO}_2$ with different internal space scales (a, b) and outer mesoporous silica shell thickness (c, d)

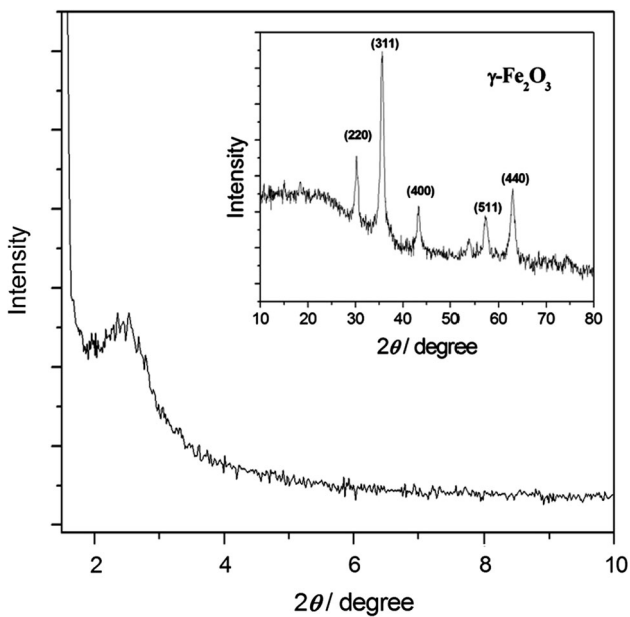
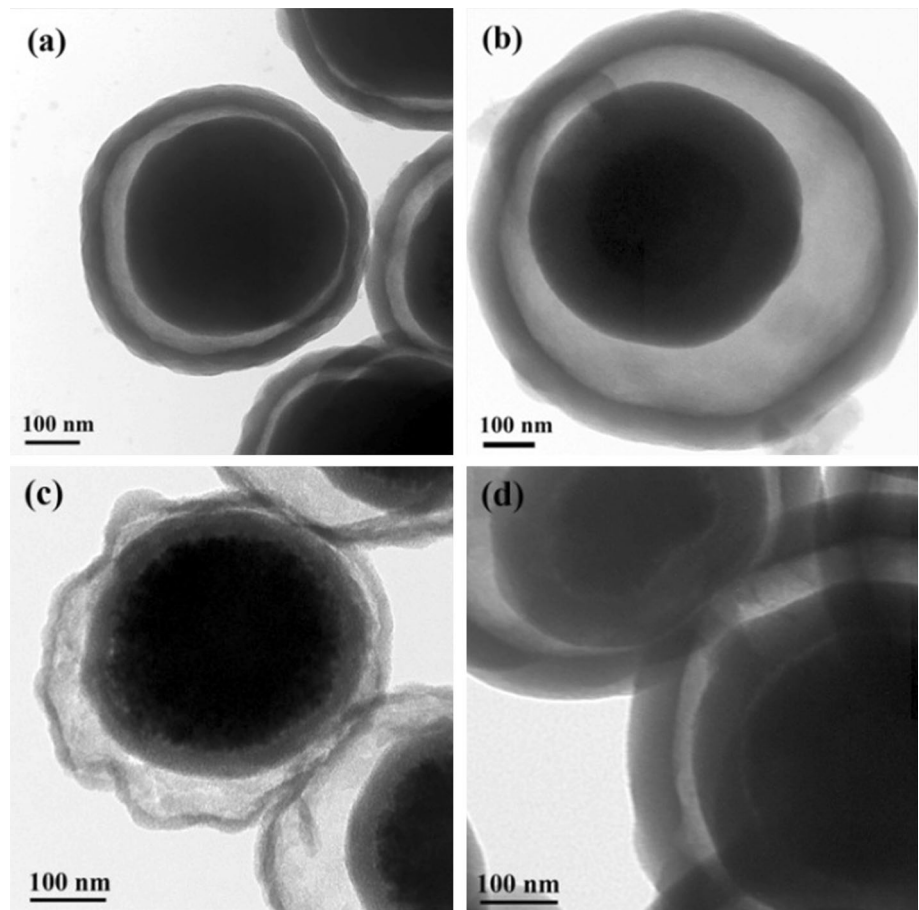


Fig. 5 Small- and wide (*inset*)-angle XRD patterns of $\gamma\text{-Fe}_2\text{O}_3@ \text{SiO}_2\text{-@mSiO}_2$

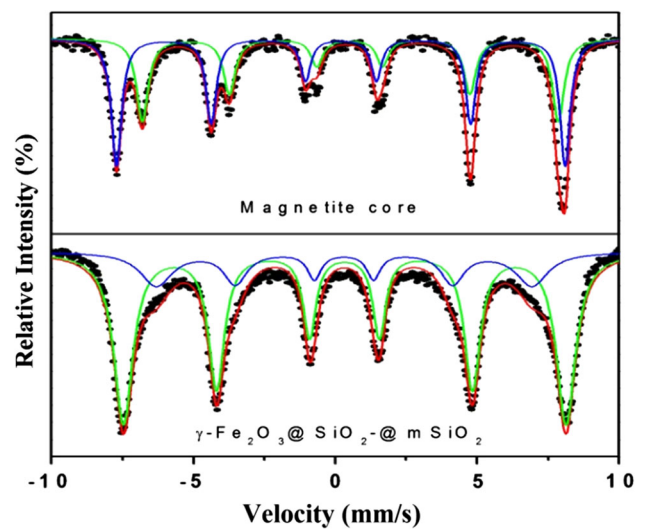
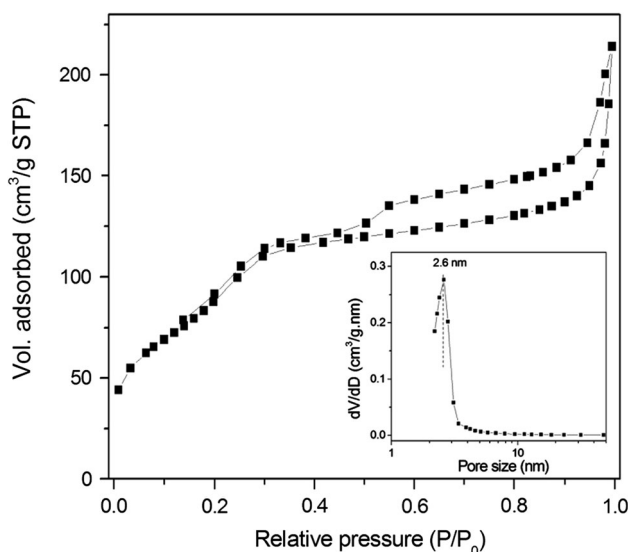


Fig. 6 Room-temperature ^{57}Fe Mössbauer spectrum of magnetite core and $\gamma\text{-Fe}_2\text{O}_3@ \text{SiO}_2\text{-@mSiO}_2$

Table 1 Mössbauer hyperfine parameters of magnetite core and γ -Fe₂O₃@SiO₂-@mSiO₂

Sample	IS (mm/s)	QS (mm/s)	B (T)	A (%)	Component
Magnetite core	0.63	0.02	45	43	Fe ^{2.5+}
	0.31	-0.02	49	57	Fe ³⁺
γ -Fe ₂ O ₃ @SiO ₂ -@mSiO ₂	0.33	0	48	75	Fe ³⁺
	0.31	0	41	25	Fe ³⁺

IS isomer shift relative to α -Fe, QS quadrupole splitting, B magnetic field, A relative subspectral area

**Fig. 7** N₂ physical adsorption/desorption isotherm and pore size distribution (*inset*) of γ -Fe₂O₃@SiO₂-@mSiO₂

similar structure and morphology to γ -Fe₂O₃@SiO₂@RF, but a slightly rough outer surface. With the removal of RF middle layer by calcination, the obtained γ -Fe₂O₃@SiO₂-@mSiO₂ exhibits obvious rattle-type structure composed of nonporous silica protecting magnetic core and hollow mesoporous silica outer shell with thickness of about 30 nm (Fig. 3a, b). SEM images also confirm the near-spherical morphology and the rattle-type architecture of γ -Fe₂O₃@SiO₂-@mSiO₂ (Fig. 3c, d). According to our previous report, the thickness of RF polymer shell of γ -Fe₂O₃@SiO₂@RF can be facily adjusted by changing the dosage of resorcinol and formaldehyde [27]. Consequently, γ -Fe₂O₃@SiO₂-@mSiO₂ with varied internal space can be obtained by using sacrificed template at different scales. The thickness of outer mesoporous silica shell can also be adjusted from 15 to 50 nm by changing the amount of TEOS (Fig. 4).

Figure 5 shows the small- and wide-angle XRD patterns of γ -Fe₂O₃@SiO₂-@mSiO₂. The small-angle XRD pattern exhibits a single weak peak centered at 2.4°, which can be attributed to the 100 reflections of MCM-41-type mesoporous silica materials, indicating that γ -Fe₂O₃@SiO₂-@mSiO₂ contains slightly ordered mesoporous structure,

but with relative lower-order degree. The diffraction peaks at wide-angle region are assigned to typical γ -Fe₂O₃ phase. Nevertheless, considering the similar XRD patterns of Fe₃O₄ and γ -Fe₂O₃, ⁵⁷Fe Mössbauer spectroscopy was used to further identify the phase of iron oxides. As shown in Fig. 6, both the initial magnetite core and final γ -Fe₂O₃@SiO₂-@mSiO₂ product present Mössbauer spectra comprising two sextet subspectra. The difference is that the magnetite core gives a subspectrum with isomer shifts of 0.63 mm/s (Table 1), indicating the existence of Fe^{2.5+} oxidation state. By contrast, γ -Fe₂O₃@SiO₂-@mSiO₂ possesses sextet spectrum with isomer shift of 0.31 and 0.33 mm/s, which refers to the single Fe³⁺ valent state and further confirms that the inner core of the composite is maghemite phase [16, 27, 28]. Such result reveals that the oxidation of initial magnetite core is unavoidable during the followed treatment. Not only during the calcination, the oxidation takes place even in silica and RF polymer-coating process [16, 26]. Figure 7 displays the N₂ physical adsorption/desorption isotherm and pore size distribution of the composite. Obviously, the material exhibits type-IV isotherm relating to the outer mesoporous silica shell with pore size centered at 2.6 nm. The abrupt increase of adsorption and hysteresis at high relative pressure region can be due to the existence of hollow interior.

3.2 Adsorption of MB

Removal of MB dye from aqueous solution was utilized to evaluate the adsorption ability of γ -Fe₂O₃@SiO₂-@mSiO₂ composite. Figure 8a shows that the γ -Fe₂O₃@SiO₂-@mSiO₂ exhibits around 70 % MB removal rate within 10 min for the dye solution with initial MB concentration of 8 mg/L, which is close to conventional mesoporous MCM-41. However, it should be noted that the both the specific surface area and pore volume of γ -Fe₂O₃@SiO₂-@mSiO₂ (329 m²/g, 0.33 cm³/g) are lower than that of MCM-41 (834 m²/g, 0.88 cm³/g). Therefore, the hollow structure of rattle-type nanocomposite should play a key role on its adsorption ability [23]. The effects of initial concentration and pH value of dye solution on the adsorption amount onto the nanocomposite were also investigated. With the increasing of initial MB concentration from 8 to 100 mg/L, the adsorption amount increased

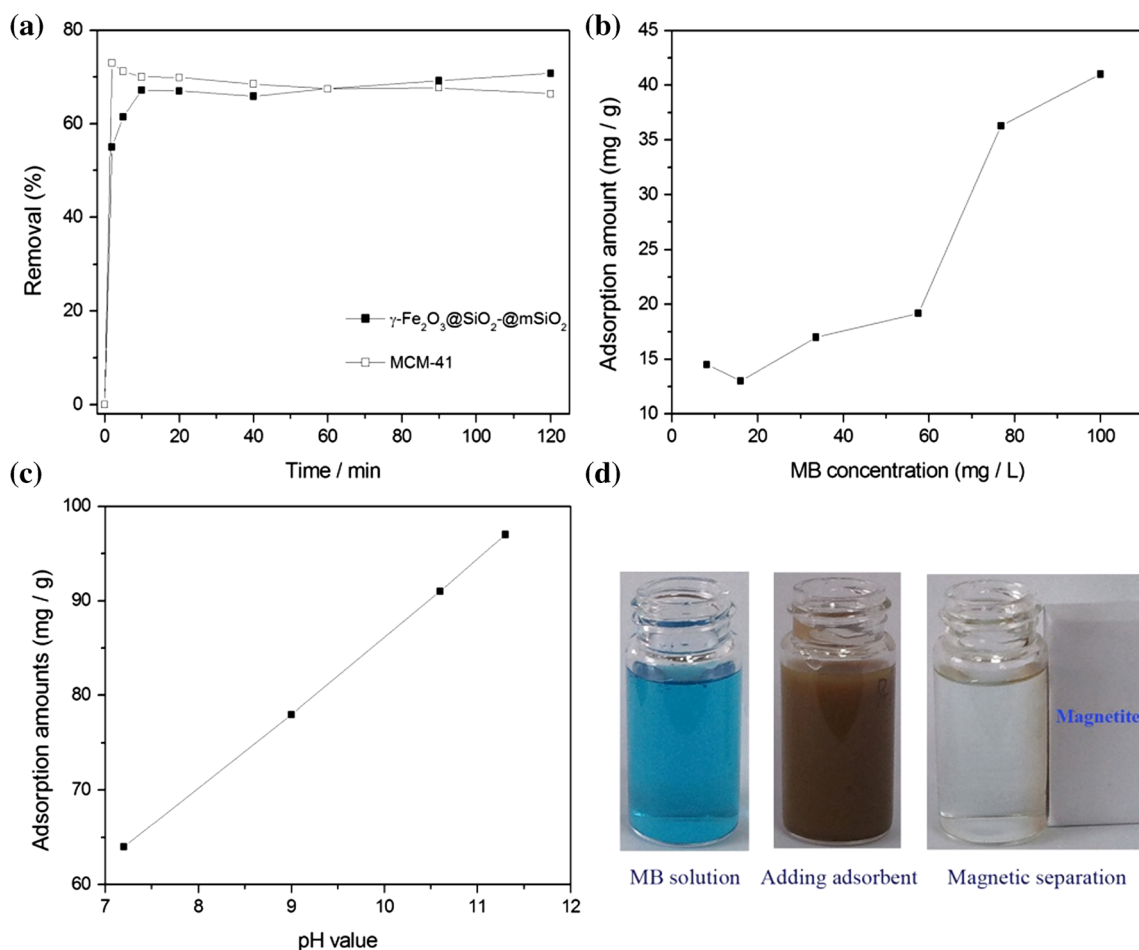
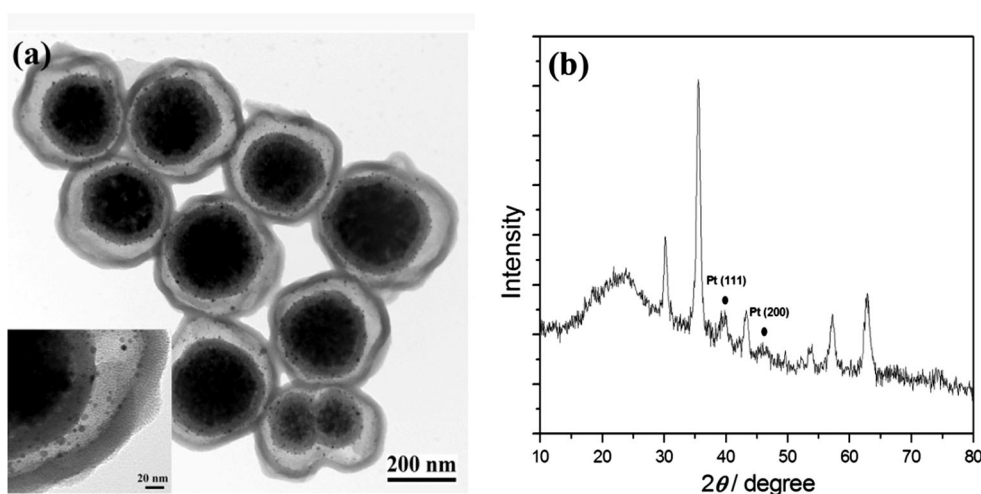


Fig. 8 **a** MB removal rate as a function of adsorption time over $\gamma\text{-Fe}_2\text{O}_3\text{@SiO}_2\text{-@mSiO}_2$ and MCM-41 (MB initial concentration = 8 mg/L, pH = 7.2), **b** effect of MB initial concentration on $\gamma\text{-Fe}_2\text{O}_3\text{@SiO}_2\text{-@mSiO}_2$ adsorption capability (pH = 7.2), **c** effect

of pH value on $\gamma\text{-Fe}_2\text{O}_3\text{@SiO}_2\text{-@mSiO}_2$ adsorption capability (MB initial concentration = 40 mg/L), **d** photos described the magnetic separation of $\gamma\text{-Fe}_2\text{O}_3\text{@SiO}_2\text{-@mSiO}_2$ after adsorption for MB

Fig. 9 TEM image **(a)** and XRD pattern **(b)** of $\gamma\text{-Fe}_2\text{O}_3\text{@SiO}_2\text{-Pt@mSiO}_2$ catalyst. *Inset* partial enlarged TEM image



from 14 to 41 mg/g (Fig. 8b), which can be due to the enhancement of interaction between MB and adsorbent [29]. The adsorption capacity also increased with the pH

value of solution (Fig. 8c), which is attributed to the negative charge of adsorbent surface formed in high-pH condition which can improve the electrostatic interaction with

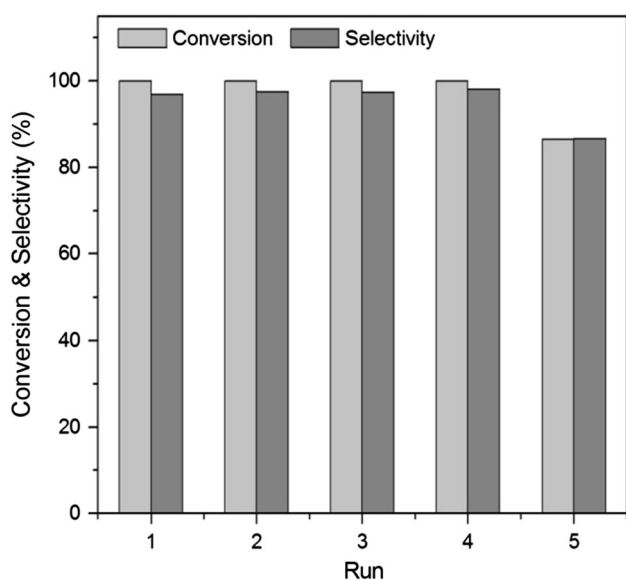


Fig. 10 Catalytic results of $\gamma\text{-Fe}_2\text{O}_3\text{@SiO}_2\text{-Pt@mSiO}_2$ catalyst for selective hydrogenation of nitrobenzol

cationic MB dye [29, 30]. For the existence of magnetic core, the nanocomposites can be facilely separated from the solution with the help of magnetic field (Fig. 8d).

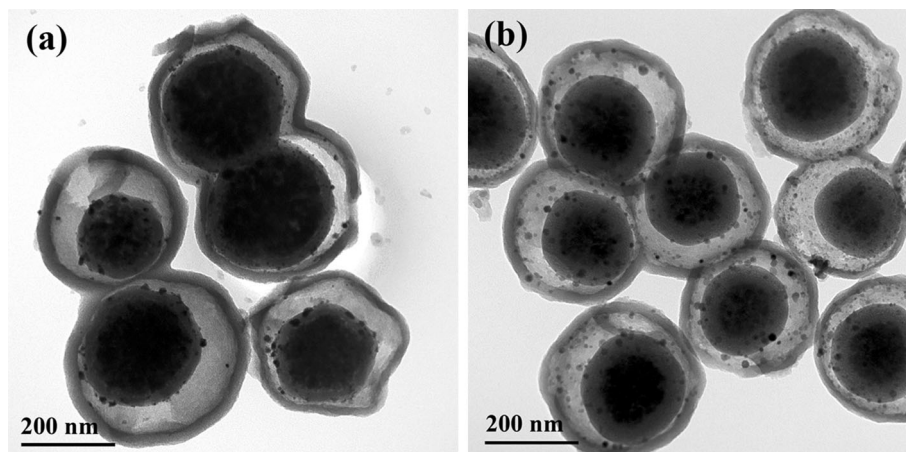
3.3 Catalytic application

The unique rattle-type architecture of $\gamma\text{-Fe}_2\text{O}_3\text{@SiO}_2\text{-@mSiO}_2$ can be used as container for active metallic nanoparticles, such as Pt, to construct composite catalytic system. Figure 9 presents the TEM image and XRD pattern of the prepared catalyst system of Pt encapsulated in $\gamma\text{-Fe}_2\text{O}_3\text{@SiO}_2\text{-@mSiO}_2$. As TEM image has shown (Fig. 9a), there are many Pt nanoparticles in the hollow space of $\gamma\text{-Fe}_2\text{O}_3\text{@SiO}_2\text{-@mSiO}_2$ locating at either the silica-coated magnetic core or the mesoporous shell. In addition, all the Pt nanoparticles are uniform in size of

5.8 ± 2.2 nm, which indicates that RF-removed calcination and followed reduction process did not lead to obvious aggregation of Pt nanoparticles. Except the diffraction peaks of $\gamma\text{-Fe}_2\text{O}_3$ core, the XRD pattern of the catalytic system (Fig. 9b) shows additional characteristic peaks at 39.8° and 46.3° , which can be indexed to (111) and (200) planes of cubic Pt crystal system, respectively, further demonstrating the existence of active Pt nanoparticles in the designed composite catalytic system.

The catalytic hydrogenation of nitroarenes is an environmentally friendly process for the production of anilines, which are important intermediates for agrochemicals, manufacturing, pharmaceuticals, and so on. Herein, the catalytic performance of the constructed catalyst was investigated by selective hydrogenation of nitrobenzene to aniline. The reaction results are showed in Fig. 10. It can be found that $\gamma\text{-Fe}_2\text{O}_3\text{@SiO}_2\text{-Pt@mSiO}_2$ is very active for this reaction, giving extreme high conversion (>99 %) and high selectivity (97 %). In addition, the catalyst exhibits prominent reusability and maintaining the excellent catalytic property in four reaction cycles. The fifth cycle showed a little drop in conversion and selectivity but still maintains a higher level (>85 %). The TEM image (Fig. 11a) reveals that the size of Pt nanoparticles of the catalyst after five cycles (8.4 ± 3.3 nm) are bigger than fresh one, which indicates that the active Pt nanoparticles tend to aggregate with each other during the reaction and lead to the activity decline. The composite catalytic system composed of Pt nanoparticles encapsulated in $\gamma\text{-Fe}_2\text{O}_3\text{@SiO}_2\text{-@mSiO}_2$ is of significant anyway. It possesses not only high activity but also excellent reusability for selective hydrogenation of nitroarenes. In addition, other active metal, such as Pd, can also be introduced into rattle-type $\gamma\text{-Fe}_2\text{O}_3\text{@SiO}_2\text{-@mSiO}_2$ to construct corresponding composite catalytic system (Fig. 11b). In general, the composite catalysts with rattle-type architecture can be described as “nanoreactor” and exhibit special catalytic

Fig. 11 TEM images of **a** $\gamma\text{-Fe}_2\text{O}_3\text{@SiO}_2\text{-Pt@mSiO}_2$ after five cycles of reaction and **b** $\gamma\text{-Fe}_2\text{O}_3\text{@SiO}_2\text{-Pd@mSiO}_2$



performances in some reactions [5, 6, 31–37]. Therefore, fabrications for the catalytic systems based on γ -Fe₂O₃@SiO₂-@mSiO₂ and exploring their catalytic applications in other reactions need to be further researched.

4 Conclusions

In summary, rattle-type magnetic silica composite with nonporous silica-coating magnetic iron oxide encapsulated in mesoporous silica hollow sphere had been prepared through a simple hard-template method. The textural parameters of the composite can be adjusted by controlling the synthesis conditions. The fabricated magnetic composite with such unique architecture can be utilized in adsorption removal of dye from aqueous solution. In addition, active metallic nanoparticles can be introduced into the composite to construct integrated catalytic system. The designed Pt-based catalyst exhibits high activity and selectivity and excellent reusability in selective hydrogenation of nitrobenzol to aniline.

Acknowledgments This work is supported by National Natural Science Foundation of China (Nos. 21403220, 21476232, 11205160).

References

- Kim SS, Zhang WZ, Pinnavaia TJ (1998) *Science* 282:1302–1305
- Zhang AF, Zhang YC, Xing N, Hou KK, Guo XW (2009) *Chem Mater* 21:4122–4126
- Zhao WR, Lang MD, Li YS, Li L, Shi JL (2009) *J Mater Chem* 19:2778–2783
- Bañ L, Bártová B, Arduini M, Mancin F (2009) *Chem Commun* 48:7584–7586
- Zhang Q, Zhang TR, Ge JP, Yin YD (2008) *Nano Lett* 8:2867–2871
- Liu C, Li JS, Qi JW, Wang J, Luo R, Shen JY, Sun XY, Han WQ, Wang LJ (2014) *ACS Appl Mater Interfaces* 6:13167–13173
- Tan LF, Liu TL, Li LL, Liu HY, Wu XL, Gao FP, He XL, Meng XW, Chen D, Tang FQ (2013) *RSC Adv* 3:5649–5655
- Yu JG, Le Y, Cheng B (2012) *RSC Adv* 2:6784–6791
- Qiang L, Meng XW, Li LL, Chen D, Ren XL, Liu HY, Ren J, Fu CH, Liu TL, Gao FP, Zhang YQ, Tang FQ (2013) *Chem Commun* 49:7902–7904
- Du L, Liao SJ, Khatib HA, Stoddart JF, Zink JI (2009) *J Am Chem Soc* 131:15136–15142
- Zhang L, Qiao SZ, Jin YG, Yang HG, Budihartono S, Stahr F, Yan ZF, Wang XL, Hao ZP, Lu GQ (2008) *Adv Funct Mater* 18:3203–3212
- Zhu YF, Fang Y, Kaskel S (2010) *J Phys Chem C* 114:16382–16388
- Yang PP, Quan ZW, Hou ZY, Li CX, Kang XJ, Cheng ZY, Lin J (2009) *Biomaterials* 30:4786–4795
- Ruiz-Hernández E, López-Noriega A, Arcos D, Izquierdo-Barba I, Terasaki O, Vallet-Regí M (2007) *Chem Mater* 19:3455–3463
- Chen Y, Chen HR, Zeng DP, Tian YB, Chen F, Feng JW, Shi JL (2010) *ACS Nano* 4:6001–6013
- Jin CZ, Wang YJ, Wei HS, Tang HL, Liu X, Lu T, Wang JH (2014) *J Mater Chem A* 2:11202–11208
- Deng YH, Cai Y, Sun ZK, Liu J, Liu C, Wei J, Li W, Liu C, Wang Y, Zhao DY (2010) *J Am Chem Soc* 132:8466–8473
- Alam S, Anand C, Ariga K, Mori T, Vinu A (2009) *Angew Chem Int Ed* 48:7358–7361
- Liong M, Angelos S, Choi E, Patel K, Stoddart JF, Zink JI (2009) *J Mater Chem* 19:6251–6257
- Kim J, Kim HS, Lee N, Kim T, Kim H, Yu T, Song IC, Moon WK, Hyeon T (2008) *Angew Chem Int Ed* 47:8438–8441
- Zhang L, Qiao SZ, Jin YG, Chen ZG, Gu HC, Lu GQ (2008) *Adv Mater* 20:805–809
- Lan F, Hu H, Jiang W, Liu KX, Zeng XB, Wu Y, Gu ZW (2012) *Nanoscale* 4:2264–2267
- Zhao WR, Chen HR, Li YS, Li L, Lang MD, Shi JL (2008) *Adv Funct Mater* 18:2780–2788
- Zhu YF, Kockrick E, Ikoma T, Hanagata N, Kaskel S (2009) *Chem Mater* 21:2547–2553
- Yue Q, Zhang Y, Wang C, Wang XQ, Sun ZK, Hou XF, Zhao DY, Deng YH (2015) *J Mater Chem A* 3:4586–4594
- Liu J, Sun ZK, Deng YH, Zou Y, Li CY, Guo XH, Xiong LQ, Gao Y, Li FY, Zhao DY (2009) *Angew Chem Int Ed* 48:5875–5879
- Jin CZ, Wang YJ, Tang HL, Wei HS, Liu X, Wang JH (2014) *J Phys Chem C* 118:25110–25117
- Zhao KF, Qiao BT, Zhang YJ, Wang JH (2013) *Chin J Catal* 34:1386–1394
- Peng XM, Huang DP, Odoom-Wubah T, Fu DF, Huang JL, Qin QD (2014) *J Colloid Interface Sci* 430:272–282
- Eftekhari S, Habibi-Yangjeh A, Sohrabnezhad SH (2010) *J Hazard Mater* 178:349–355
- Liu J, Yang HQ, Kleitz F, Chen ZG, Yang TY, Strounina E, Lu GQ, Qiao SZ (2012) *Adv Funct Mater* 22:591–599
- Lee J, Park JC, Song H (2008) *Adv Mater* 20:1523–1528
- Yin YD, Rioux RM, Erdonmez CK, Hughes S, Somorjai GA, Alivisatos AP (2004) *Science* 304:711–714
- Ikeda S, Ishino S, Harada T, Okamoto N, Sakata T, Mori H, Kuwabata S, Torimoto T, Matsumura M (2006) *Angew Chem Int Ed* 45:7063–7066
- Arnal PM, Comotti M, Schüth F (2006) *Angew Chem Int Ed* 45:8224–8227
- Li J, Zeng HC (2005) *Angew Chem Int Ed* 44:4342–4345
- Yang Y, Liu X, Li XB, Zhao J, Bai SY, Liu J, Yang QH (2012) *Angew Chem Int Ed* 51:9164–9168